NAVAL POSTGRADUATE SCHOOL

MONTEREY, CALIFORNIA

THESIS

FABRICATION AND OPTIMIZATION OF CARBON NANOMATERIAL-BASED LITHIUM ION BATTERY ANODES

by

Parina Somnhot

March 2012

Thesis Advisor:	Sebastian Osswald
Second Reader:	Joseph Farmer

Approved for public release; distribution is unlimited

THIS PAGE INTENTIONALLY LEFT BLANK

REPORT DOCUMENTATION PAGE		Form Approved OMB No. 0704–0188

1. AGENCY USE ONLY *(Leave blank)*	2. REPORT DATE	3. REPORT TYPE AND DATES COVERED
	March 2012	Master's Thesis

4. TITLE AND SUBTITLE Fabrication and Optimization of Carbon Nanomaterial-Based Lithium-Ion Battery Anodes	5. FUNDING NUMBERS
6. AUTHOR(S) Parina Somnhot	
7. PERFORMING ORGANIZATION NAME(S) AND ADDRESS(ES) Naval Postgraduate School Monterey, CA 93943–5000	8. PERFORMING ORGANIZATION REPORT NUMBER
`	10. SPONSORING/MONITORING AGENCY REPORT NUMBER

11. SUPPLEMENTARY NOTES The views expressed in this thesis are those of the author and do not reflect the official policy or position of the Department of Defense or the U.S. Government. IRB Protocol number ___N/A____.

12a. DISTRIBUTION / AVAILABILITY STATEMENT	12b. DISTRIBUTION CODE
Approved for public release; distribution is unlimited	

13. ABSTRACT (maximum 200 words)

Lithium-ion batteries possess high energy and power densities, making them ideal candidates for energy storage requirements in various military applications. Commercially produced lithium-ion battery anodes are commonly graphitic carbon-based. However, graphitic carbons are limited in surface area and possess slow intercalation kinetics. The energy and power density demands of future technologies require improved lithium-ion battery performance.

Carbon nanomaterials, such as carbide-derived carbons, carbon onions and carbon nanotubes, used in lithium-ion battery electrodes can exhibit a much higher specific capacity (up to 1000 mAh/g) and faster charge/discharge characteristics than their graphitic carbon counterpart, which has a specific capacity of 372 mAh/g. However, little is known about how certain characteristics, such as structure and surface chemistry, for example, of carbon nanomaterials affect the electrochemical performance of lithium-ion batteries. Further investigation is necessary to fully understand the governing storage mechanism. A comprehensive analysis of the electrochemical performance of new anode materials, which includes a wide range of tests, requires the ability to fabricate a large number of electrodes and batteries of nearly identical quality. Thus, the optimization of the individual cell production steps is a crucial requirement for a comprehensive study of the electrochemical properties of new anode materials and is central to this research.

14. SUBJECT TERMS Lithium-Ion Batteries, Amorphous Carbon, Carbide-Derived Carbon, Carbon Onions, Carbon Nanotubes, Multi-Walled Carbon Nanotubes	15. NUMBER OF PAGES 71
	16. PRICE CODE

17. SECURITY CLASSIFICATION OF REPORT	18. SECURITY CLASSIFICATION OF THIS PAGE	19. SECURITY CLASSIFICATION OF ABSTRACT	20. LIMITATION OF ABSTRACT
Unclassified	Unclassified	Unclassified	UU

THIS PAGE INTENTIONALLY LEFT BLANK

Approved for public release; distribution is unlimited

FABRICATION AND OPTIMIZATION OF CARBON NANOMATERIAL-BASED LITHIUM-ION BATTERY ANODES

Parina Somnhot
Lieutenant, United States Navy
B.S., Boston University, 2005

Submitted in partial fulfillment of the
requirements for the degree of

MASTER OF SCIENCE IN MECHANICAL ENGINEERING

from the

NAVAL POSTGRADUATE SCHOOL
March 2012

Author: Parina Somnhot

Approved by: Sebastian Osswald
Thesis Advisor

Joseph Farmer
Second Reader

Knox T. Millsaps
Chair, Department of Mechanical Engineering

THIS PAGE INTENTIONALLY LEFT BLANK

ABSTRACT

Lithium-ion batteries possess high energy and power densities, making them ideal candidates for energy storage requirements in various military applications. Commercially produced lithium-ion battery anodes are commonly graphitic carbon-based. However, graphitic carbons are limited in surface area and possess slow intercalation kinetics. The energy and power density demands of future technologies require improved lithium-ion battery performance.

Carbon nanomaterials, such as carbide-derived carbons, carbon onions and carbon nanotubes, used in lithium-ion battery electrodes can exhibit a much higher specific capacity (up to 1000 mAh/g) and faster charge/discharge characteristics than their graphitic carbon counterpart, which has a specific capacity of 372 mAh/g. However, little is known about how certain characteristics, such as structure and surface chemistry, for example, of carbon nanomaterials affect the electrochemical performance of lithium-ion batteries. Further investigation is necessary to fully understand the governing storage mechanism. A comprehensive analysis of the electrochemical performance of new anode materials, which includes a wide range of tests, requires the ability to fabricate a large number of electrodes and batteries of nearly identical quality. Thus, the optimization of the individual cell production steps is a crucial requirement for a comprehensive study of the electrochemical properties of new anode materials and is central to this research.

THIS PAGE INTENTIONALLY LEFT BLANK

TABLE OF CONTENTS

THIS PAGE INTENTIONALLY LEFT BLANK

LIST OF FIGURES

THIS PAGE INTENTIONALLY LEFT BLANK

LIST OF TABLES

THIS PAGE INTENTIONALLY LEFT BLANK

LIST OF ACRONYMS AND ABBREVIATIONS

2H	Hexagonal
3R	Rhombohedral
CDC	Carbide-Derived Carbon
CMC	Carboxymethyl Cellulose
CNT	Carbon Nanotubes
DMC	Dimethyl Carbonate
EC	Ethylene Carbonate
EMC	Ethyl Methyl Carbonate
HRTEM	High-Resolution Transmission Electron Microscopy
MWCNT	Multi-Walled Carbon Nanotubes
ND	Nanodiamond
PE	Polyethylene
PP	Polypropylene
PVDF	Polyvinylidene Fluoride
SEI	Solid Electrolyte Interphase
SWCNT	Single-Walled Carbon Nanotubes

THIS PAGE INTENTIONALLY LEFT BLANK

ACKNOWLEDGMENTS

My thesis advisor, Dr. Sebastian Osswald, deserves the most recognition for offering solid direction when I needed it most. Aside from the countless whiteboard lessons and calculations, he taught me how to embrace the less-desirable results as part of the research process instead of discouragement. He is a phenomenal teacher, mentor and advisor and possesses an endless supply of patience.

I would also like to thank Dr. Joseph Farmer for inspiring me to conduct this research. None of it would have been possible without his extended chemistry lessons during his Energy Conversion and Storage course and his extra encouragement when I started to doubt myself. He constantly reminded me what I should take from my experience at Naval Postgraduate School.

I also spent many long hours in the laboratory with Kamryn Sakamoto, whose dedication in establishing battery research capabilities at Naval Postgraduate School made this continuation of her work much easier than it could have been. It is difficult to find an engineer and friend of her caliber.

THIS PAGE INTENTIONALLY LEFT BLANK

I. INTRODUCTION

A. DEVELOPMENT OF ENERGY STORAGE TECHNOLOGY

The challenge of developing clean, efficient energy solutions has influenced the direction of everything from foreign policy to national security. There is an increasing emphasis on reducing reliance on a quickly depleting supply of fossil fuels and cultivating alternative energy solutions, such as wind and solar power. However, the need for consistent, sustainable energy technology not subject to the unpredictability of nature requires further advancement in energy conversion and storage. Thus, the pursuit of a balance between energy efficient solutions and environmentally friendly solutions is dictating the course of energy technology.

As suggested with the advent of the Great Green Fleet Carrier Strike Force, the United States Navy has a particular interest in improving energy storage technology. The Navy has recently experimented with alternative energy resources from biodiesel in aircraft and surface ships to more recently, algae in its landing craft [1]. All types of equipment from communications to complex combat systems electronics are powered or reinforced with secondary, or rechargeable, lithium-ion battery sources. What if there was a means to harness more energy in those batteries by utilizing advanced storage materials? The savings from energy storage life and the preservation of resources would prove invaluable.

The United States Navy's use of electrochemical energy storage, particularly in secondary batteries, uses the same concept as secondary batteries for general applications. Each battery contains an anode, a cathode, a separator between the two, an electrolyte and a containment apparatus. While charging, chemical reactions at the anode and cathode are driven by an external

voltage applied across the electrodes. During discharge, the chemical reactions are reversed, and electrons flow through an external circuit, creating electrical energy [2].

There are several characteristics of secondary batteries that are used to measure their performance, including power density, energy density, cycle life and stability. The choice of electrode material has the most impact on these characteristics, and electrode material is typically chosen based on its specific capacity and specific energy. However, materials with the most specific capacity may not be practical for different applications. For instance, oxygen is a very energy dense cathode material in relatively high abundance, making it ideal for applications using metal-air batteries. However, in fuel cells used in unmanned underwater vehicles, the challenge to store both oxygen and hydrogen in a safe, economical and easily accessible fashion requires a more robust design.

Additionally, one must achieve a balance between energy density, or how much energy a device can store, and power density, how easy it is to access the energy, or more specifically, the rate at which free lithium ions can be absorbed and emitted. For the sake of comparison, a Ragone chart (Figure 1) is used to illustrate how different energy storage devices rank amongst their counterparts.

As depicted in Figure 1, fuel cells lie on one end of the spectrum. They yield a very high energy density and are desirable for applications requiring a device capable of storing a high amount of energy. Their power output, however, is relatively low. Capacitors, on the other hand, allow for nearly instantaneous access to energy but are not capable of storing the energy for very long. Lithium-based batteries offer a desirable balance between the two. They offer slightly higher energy density than their lead-acid and nickel-cadmium counterparts and a high power density, making lithium-based batteries a popular choice in a variety of applications [3].

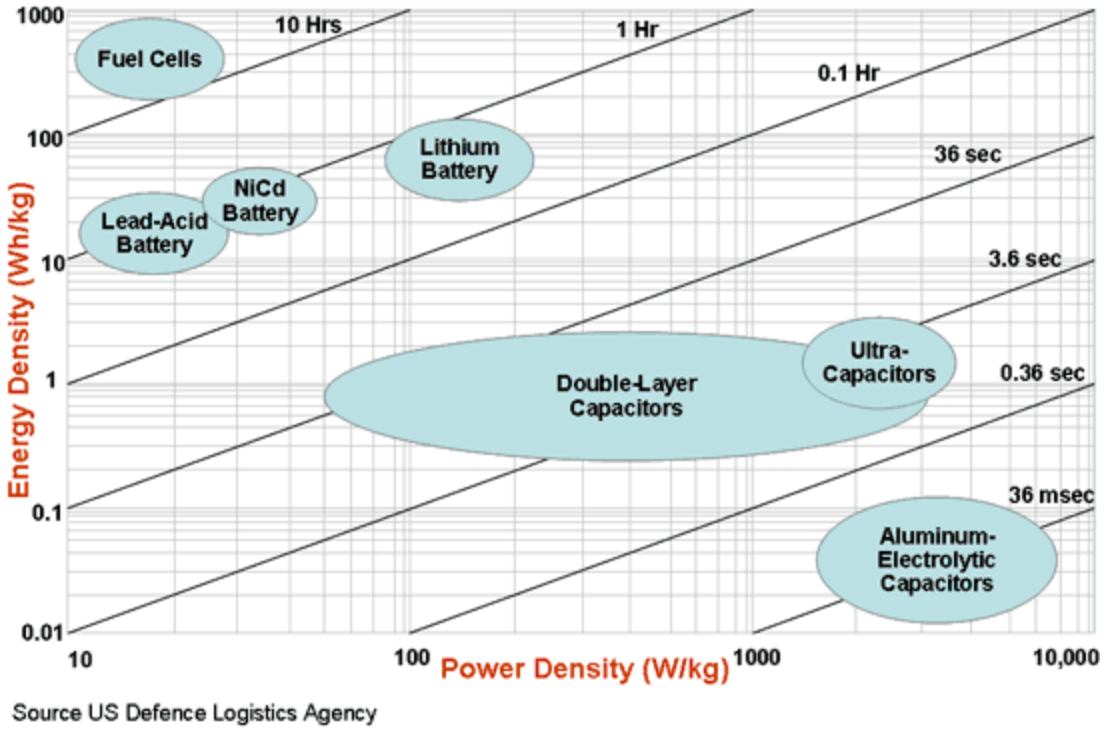

Figure 1. A Ragone plot compares the performance of a wide range of electrochemical devices based on energy density and power density. Capacitors yield a lot of power but are limited in they can store. Fuel cells can store a high amount of energy but yield a low power output. Lithium-based batteries a desirable balance between energy density and power density (From [3]).

B. LITHIUM-ION BATTERIES

1. Overview

Although the shape and size of a lithium-ion battery depends on its application, the internal components of a lithium-ion battery are generally the same. There may be small material variations between coin cells, prismatic cells, pouch cells and cylindrical cells, but the structure of the battery does not change.

2. Design

Generally, lithium-ion batteries consist of an anode, a cathode, a separator and electrolyte. The anode and cathode materials exist in powder forms, and the electrodes are a mixture of active material, binder and conductive carbon additive.

A polymeric binder, such as polyvinylidene fluoride (PVDF), helps the anode and cathode powders adhere to a metal foil current collector. Copper is typically used for the negative electrode, the anode. The cathode, or positive electrode, uses an aluminum current collector [4]. The negative and positive electrodes are separated by a liquid electrolyte-soaked, ion-conducting microporous polyethylene (PE) or polypropylene (PP) film. Some of the more advanced lithium-ion battery technologies contain gel-polymer or solid-state electrolytes [5].

As shown in Figure 2, the anode and cathode of a cylindrical lithium-ion cell are partitioned by a polymeric separator through which lithium ions travel during charge and discharge. The separator prevents contact between the anode and cathode and subsequent shorting. Electrons flow in the outer circuit.

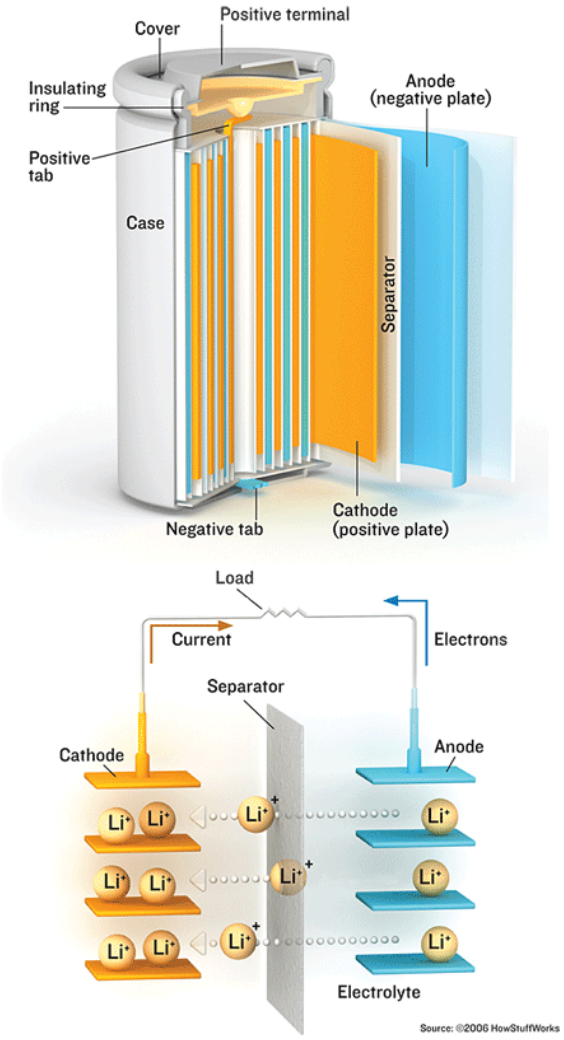

Figure 2. A cylindrical lithium-ion cell. Lithium ions flow between anode and cathode through the separator and electrolyte upon charge and discharge. Electrons flow through the outer circuit (From [6]).

During discharge, lithium ions flow from the negative electrode to the positive electrode through the separator and electrolyte. Electrons flow the opposite way through the outer circuit, powering a device. Once all the lithium ions have traveled across the separator, the cell is fully discharged. The reverse is true upon recharging. When the lithium-ion cell is charging, current is forced into the cell, and the lithium ions flow from the positive electrode across the separator and electrolyte back to the negative electrode. Electrons flow in the

opposite direction in the outer circuit. When all the lithium ions have traveled back to the negative electrode, the cell is fully charged [6].

3. Principle of Operation

The basic principle behind the operation of a lithium-ion battery is governed by a simple oxidation-reduction chemical reaction. When charging a lithium-ion battery, the positive electrode undergoes oxidation, while the negative electrode experiences reduction. “M” in the general half-cell reactions below depicts the metal used in the lithium metal oxide [4]:

Cathode: $LiMO_2 \rightarrow Li_{1-x}MO_2 + xLi^+ + xe^-$

Anode: $C + xLi^+ + xe^- \rightarrow Li_xC$

The opposite reaction occurs upon discharge:

Cathode: $Li_{1-x}MO_2 + xLi^+ + xe^- \rightarrow LiMO_2$

Anode: $Li_xC \rightarrow C + xLi^+ + xe^-$

The layered or tunneled lattice structure of electrode materials facilitates host sites for lithium ions to intercalate during charge and discharge. The insertion and extraction of lithium ions between sites occurs reversibly without any structural changes to the lattices of the electrode materials. Graphite and layered silicates are often used as intercalation compounds in lithium-ion batteries. Graphitic compounds, in particular, have been researched extensively in the field of lithium-ion batteries, especially in alkali metal intercalation of graphite. The reversible movement of lithium ions back and forth across intercalation compounds on the anode and cathode is known as the “rocking chair mechanism” [4].

C. CARBON-BASED ELECTRODE MATERIALS

1. Graphitic Carbons

The most commonly used anode materials in lithium-ion batteries are graphitic carbon-based. Thus, the characteristics and properties of graphitic

carbons have been studied extensively. It has a theoretic specific capacity of 372 mAh/g and exhibits limited reversible capacity and relatively good cycle performance. It is also inexpensive compared to other anode materials and is available in large quantities.

The structure of graphitic carbons consists of stacked graphene layers in which the carbon atoms are arranged in a hexagonal lattice. The stacking of layers can occur in two arrangements, with most graphitic carbons consisting of a mixture of the two. Hexagonal (2H) graphite has a pattern of AB AB AB (Figure 3). Rhombohedral (3R) graphite possesses a stacking pattern of ABC ABC (Figure 4) [7].

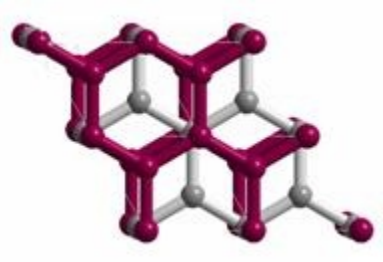

Figure 3. Hexagonal graphite with an AB AB AB stacking pattern (From [8]).

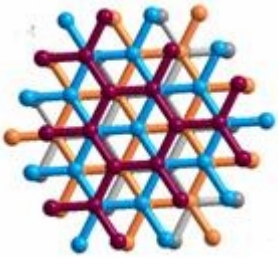

Figure 4. Rhombohedral graphite with an ABC ABC ABC stacking pattern (From [8]).

In either case, during the intercalation process, the layer stacking converts to AAA, with neighboring graphene layers aligning perfectly. Lithium ions intercalate between those layers, as seen in Figure 5.

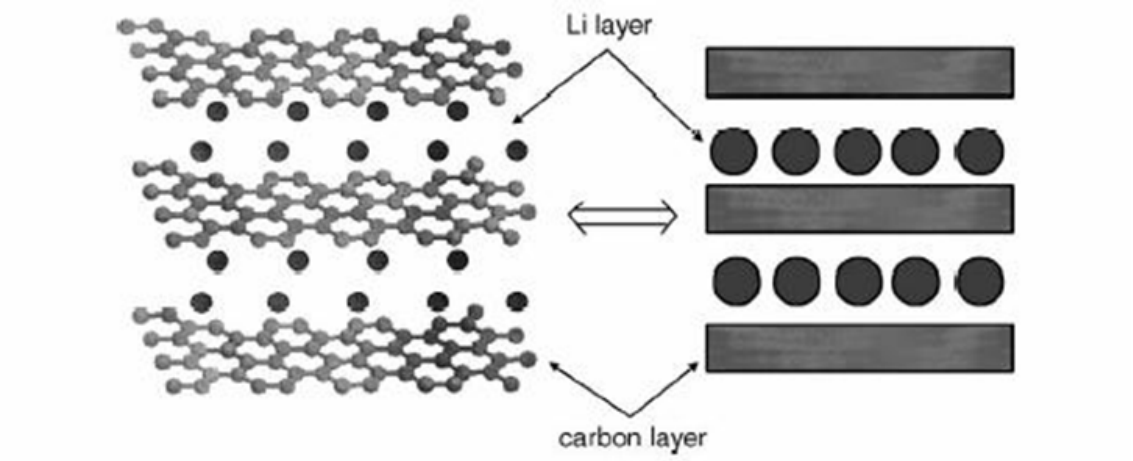

Figure 5. Intercalation of lithium ions between graphene layers of graphitic carbon (From [9]).

The lithium ions, however, do not intersperse homogeneously during intercalation and end up forming lithium-rich pockets [7]. Research has proven that allotropic modifications to the graphitic anodes have a direct impact on graphitic carbon-based anodes.

2. Disordered Carbons: Amorphous Carbons

Amorphous carbons contain small layered segments. These segments are randomly organized and often contain less than three to four layers that actually align. As shown in Figure 6, nanoporous carbide-derived carbons (CDC) are of particular interest due to their potential for higher theoretic specific capacity with decreasing crystallite thickness in the realm under 10 nm.

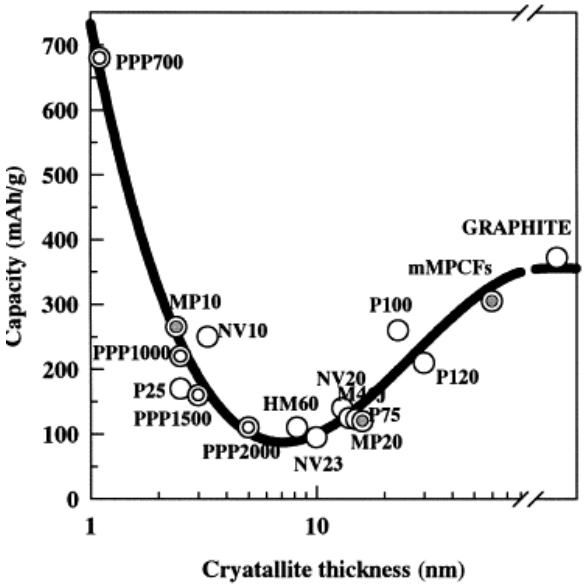

Figure 6. Specific charge capacity of the various carbon fiber and PPP-based carbon electrodes at the second cycle as a function of crystallite thickness, determined by X-ray diffraction analysis (From [9]).

CDCs range from disordered amorphous carbon to highly ordered graphitic carbon. CDCs are developed by synthesis through high-temperature chlorination, also known as halogenation, of metal carbides. Process parameters, such as chlorination temperature, pressure and choice of carbide precursor govern the final CDC structure. CDCs are typically chlorinated at temperatures between 200 and 1200 °C [10]. The chlorine gas etches the metal away, leaving a highly amorphous carbon material (Figure 7).

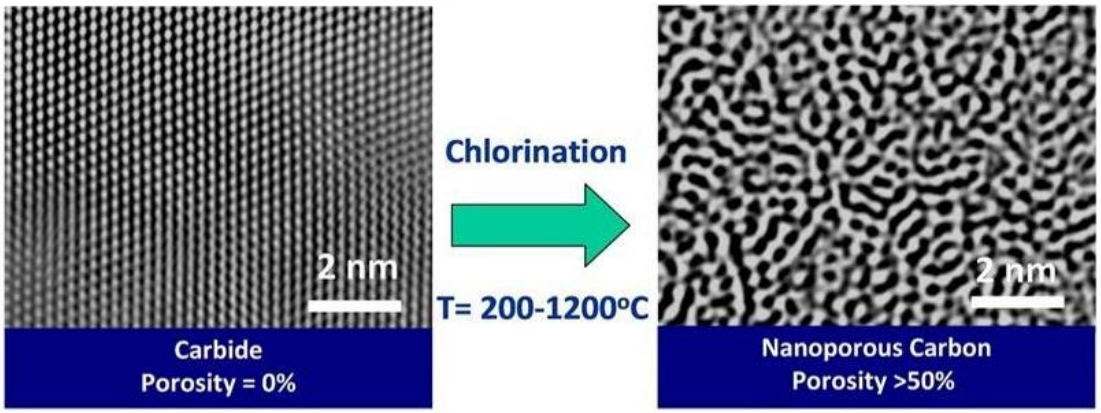

Figure 7. High-resolution transmission electron microscopy (HRTEM) image depicting the change in porosity in a metal carbide after chlorination (From [11]).

Choice of precursor material depicted in Figure 8 directly affects the distribution of pores. In this particular example, use of a Ti_3SiC_2 precursor produces a bimodal distribution of small and large pores, while use of SiC produces a more homogeneous distribution of small pores [11].

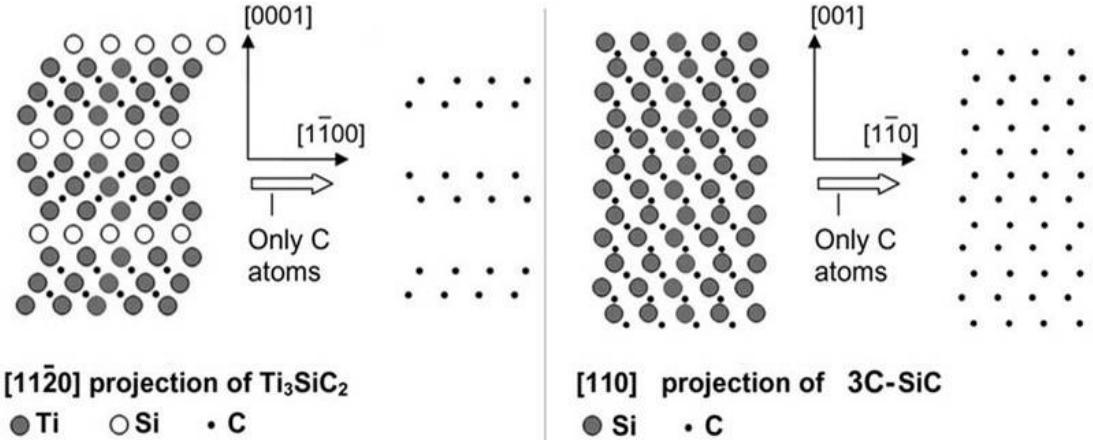

Figure 8. Effect of carbide precursor material on pore distribution (From [11]).

CDCs have the ability to precisely and homogeneously adjust surface area, degree of graphitization, crystal size and porosity, making them ideal candidates for lithium-ion battery use.

3. Other Carbon Nanomaterials

a. Carbon Onions

Other carbon nanomaterials have shown great potential for energy storage applications. The discovery of carbon onions coincided with that of carbon nanotubes (CNT), but there is much room for investigation of their properties. Interest in their use in energy storage applications continues to grow due to their unique nanostructure. They are composed of several layers of concentric, fullerene spheres stacked inside one another [12].

The advantage of using carbon onions in lithium-ion battery applications again lies in the control of final carbon onion structure using variations in synthesis methods. Although many synthesis methods for the production of carbon onions are available, the most useful for this study in lithium-ion battery energy storage involves thermal annealing of nanodiamond (ND) powders. Alternate methods yield high impurity content and far too many variations in carbon onion size. With ND powders, however, amorphous carbon and catalyst impurities are generally removed from the ND precursor. There is no additional catalyst requirement, and size distribution of the carbon onions can be easily controlled by changes to size distribution of the ND powder in the thermal annealing process, rendering the interpretation of electrochemical data more accurate and consistent [13].

b. Multi-Walled Carbon Nanotubes (MWCNT)

Carbon nanotubes (CNT) are generally classified into two groups: single-walled carbon nanotubes (SWCNT) and multi-walled carbon nanotubes (MWCNT). SWCNT contain a hollow cylindrical shape composed of a single graphene layer and demonstrate metallic or semiconductor characteristics.

MWCNT, on the other hand, are metallic in character and can have two or more concentric cylindrical layers. Amongst carbon nanostructures, SWCNT and MWCNT contain the most studies in lithium-ion battery applications. They have become a popular choice for potential replacement of graphitic carbons in lithium-ion batteries, due to contention that their inter-shell spaces, inter-tube channels and internal cores may provide additional sites for lithium storage. This particular study focuses on the use of MWCNT in lithium-ion battery electrodes based on the notion that lithium intercalation is possible in the same ways as with SWCNT and between graphene walls of individual CNT [14].

D. CURRENT CHALLENGES

Lithium-ion battery research capabilities were established at Naval Postgraduate School in 2011. By the year's end, the development and implementation of an electrode fabrication process was still in its infancy and was plagued with several problems. Although the data obtained from the initial CDC-based electrode test results was promising, physical inconsistencies from the production of electrodes continuously emerged, threatening the validity of test results and rendering any findings inconclusive [15].

One of the most significant issues outstanding from initial lithium-ion battery research at NPS included large variations in weight distribution due to inconsistencies in the casting and drying portions of the electrode production process (Figure 9).

Figure 9. Laboratory-produced electrode film using graphite. Prior to optimization, electrode films produced in the laboratory lacked homogeneity and contained large variations in weight distribution.

These excessive weight fluctuations across a single electrode called the reproducibility of the entire fabrication process into question, consequently casting doubt in test results. Although much effort had been devoted to the establishment and development of the fabrication process, the process itself lacked the standardization required to make any inferences. Most importantly, the fabrication process in place was not sufficient to enable researchers to draw any conclusions about the relationship between the electrochemical performance of carbon nanomaterials and the unique structures of those materials.

E. ThesiS objectives

The objective of this study is to standardize and optimize the fabrication process of carbon nanomaterial-based anodes for lithium-ion batteries in order to allow for higher reproducibility, improved cell quality and consistent data from characterization and testing. Increasing the reliability of the results will enable a

more conclusive evaluation of the use of carbon nanomaterial-based anodes in lithium-ion battery applications. Several steps are required to obtain this objective.

- Optimize the electrode manufacturing process such that the electrode films produced are homogeneous and of constant thickness. Prior efforts yielded excessive variations in weight distribution and composition.
- Cell fabrication must be optimized to achieve higher reproducibility in test performance. The ability to produce large quantities of laboratory-scale test batteries with similar properties is vital to accurately assessing performance of new battery materials.
- Determine the electrochemical performance of the optimized CDC electrodes and compare with self-made and commercially available graphite anodes.
- Explore the suitability of the optimized electrode fabrication process for other carbon nanomaterials, such as carbon onions and CNTs.

II. METHOD

A. MATERIALS

Lithium-ion batteries are produced in a multitude of shapes and sizes for various applications, and the production of lithium-ion batteries requires a variety of materials. For this particular research, button-type coin cells were produced. Each cell consisted of an anode, cathode, current collector, polymeric binder, separator, electrolyte, solvent and battery casing. Unless otherwise indicated, the materials used to produce these batteries were supplied by MTI Corporation.

This study used several different electrode materials. A commercially available graphite anode (specific capacity: 330 mAh/g) supplied by MTI Corporation was initially used in order to establish a baseline for subsequent research. The second series of electrodes was based on commercially available graphite powder, but electrodes were fabricated using the NPS process (assumed specific capacity: 372 mAh/g). Laboratory-produced anodes composed of CDC powder synthesized from TiC at 600 and 1200 °C (Y-Carbon Inc., USA), MWCNT (Arkema, USA) and carbon onions (obtained from Drexel University) were also used. The cathodes used in this research were comprised of commercial lithium cobalt oxide ($LiCoO_2$) or lithium metal.

The binder used during the powder preparation portion of the electrode fabrication process was PVDF, paired with N-Methyl-2-Pyrrolidone (MNP, C_5H_9NO) solvent. The current collectors were composed of aluminum and copper foil. The material used for the separator was a microporous polyolefin (thickness ~0.1 μm), paired with an electrolyte composed of 1 M $LiPF_6$ and a 1:1:1 mixture of ethylene carbonate (EC), dimethyl carbonate (DMC) and ethyl methyl carbonate (EMC). The above materials were purchased from MTI.

The stainless steel CR2032 coin cell casings consisted of a top case on the cathode side, a bottom case on the anode side, three spacers (15.4 mm X 1.1 mm) and a spring (15.8 mm X 0.5 mm).

B. ELECTRODE FABRICATION

1. Electrode Powder Preparation

Anodes fabricated in this study were composed of carbon materials in powder form, including graphite, CDC (chlorinated at 600 °C and 1200 °C), carbon onion and MWCNT. Cathodes were commercially produced $LiCoO_2$ and lithium metal. The anode fabrication process for the powders was the same, but the amount of polymer binder and conducting carbon additive varied based on the material used. The fabrication steps for electrode recipes were established in prior research at Naval Postgraduate School [15].

PVDF binder was used in the powder preparation process to bind the powder particles together. It also facilitates the adhesion to the copper current collector foil. Acetylene black, an active carbon, is used to increase the electronic conductivity of the electrode. The dry ingredients in prior research at NPS were previously ball-milled for 30 minutes using an 8000 M SPEX Sample Prep Mixer/Mill, but this step was eliminated from the process. Hand stirring the dry ingredients was sufficient to mix the powder uniformly while minimizing damage to particles.

2. Slurry Preparation and Electrode Casting

The powder mixture was added to a glass vial. NMP solvent was added in order to dissolve the PVDF binder and create a slurry. Addition of NMP solvent, which can be hazardous, was conducted under a fume hood using a glass pipette and a pipette dispenser (Figure 10a) and then stirred by hand (Figure 10b).

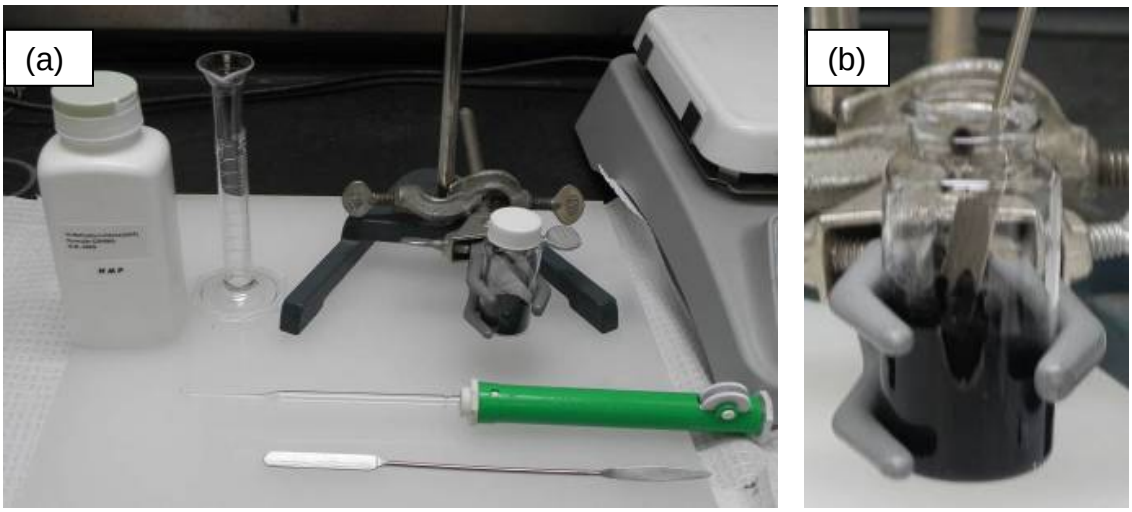

Figure 10. a) Slurry preparation setup under the fume hood with NMP solvent, glass pipette with dispenser, and the ball milled powder mixture containing LiFePO4, acetylene black, and PVDF binder; and b) Prepared slurry after adding NMP solvent to the powder mixture (From [15]).

The ratios of active material to additives varied due to differences in material density and dispersion. The slurry height during casting also varied, depending on the viscosity of the slurry. The recipes in Table 1 summarize the optimized recipes for electrode production.

Material		Additives			Height (mm)
Type	Weight (mg)	PVDF (mg)	Acetylene Black (mg)	NMP (mL)	
Graphite	1000	150	150	5.6	1
CDC 600 °C	1050	250	0	5.4	0.7
CDC 1200 °C	1050	250	0	5.4	0.7
Carbon Onion	840	155	50	5.2	1

Table 1. Optimized recipes of electrode mixtures.

The vial was then capped and sealed with paraffin wax paper before placement into the ultrasonic bath (PC3 Ultrasonic Cleaner) for a total of 30 minutes in order to dissolve the PVDF (Figure 11). Every ten minutes the slurry was also stirred by hand.

Figure 11. Ultrasonic bath. Each vial was sonicated in the ultrasonic bath for a total of 30 minutes.

During sonication, the copper current collector was flattened onto a glass plate using Kim wipes and ethanol. The current collector was then taped onto the glass and placed under the fume hood. While casting the slurry onto the current collector, the height of the slurry was controlled with a micrometer adjustable film applicator, which uses micrometer screws to vary the thickness of the electrode film.

Following sonication and additional stirring, the slurry was poured from the vial onto the current collector foil (Figure 12a). The applicator blade was pushed across the slurry to spread the slurry onto the current collector foil into a thin film (Figure 12b) of constant thickness (Figure 12c).

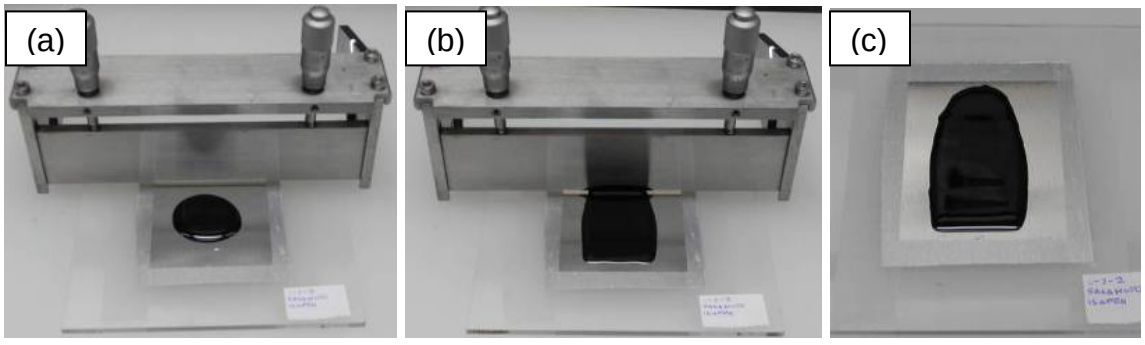

Figure 12. (a) $LiFePO_4$ slurry applied on foil current collector and (b) $LiFePO_4$ slurry casted with applicator and (c) $LiFePO_4$ casted (From [15]).

3. Battery Assembly

Then the electrode film was placed into a laboratory oven overnight at 120 °C to dry. Drying the electrode films in the laboratory oven helped prevent cracking, as electrode films dried under the fume hood experienced extensive flaking due to the continuous air flow in the fume hood.

After the electrode films dried, they were removed from the glass slide and cut with the MTI disc cutter (Figure 13).

Figure 13. MTI disc cutter used to cut individual electrodes from an electrode film.

The electrodes were then individually weighed and labeled based on their original location on the current collector foil. Weight measurements of electrodes produced across a single electrode film allowed assessment of the homogeneity of the film. Ensuring a level surface during casting and the proper viscosity of the slurry greatly reduced the weight variations across a single electrode.

The electrodes were placed in the laboratory oven overnight to remove moisture. They were then transferred to the side chamber of an argon-filled glove

box (Figure 14), where they were placed under vacuum before being transferred inside the glove box for battery assembly.

Figure 14. An Argon-filled glove box used for battery assembly. The glove box prevents moisture and oxygen from interacting with the internal battery components and reducing the cycle life of the battery (From [15]).

The small transfer chamber of the glove box was used to transfer electrodes into the glove box. Once it was secured, it was evacuated and placed under vacuum (-30 psi) for five minutes. The chamber was then filled with argon until it reached atmospheric pressure before the electrodes were transferred inside the glove box for battery assembly. The inert environment prevents moisture and oxygen contamination to the internal battery components.

Assembly of the coin cell started with the negative battery casing of the coin cell, followed by a spring and three spacers to prevent movement of components inside the coin cell. A schematic is shown in Figure 15.

Figure 15. Button-type coin cell assembly schematic (From [15]).

The anode was placed on top of the spacers with the active material facing up. Four drops of electrolyte were added to the active material side of the anode before the separator was placed on top. The top of the separator was also soaked with four drops of electrolyte before placing the cathode on top, active material side down. Lastly, the positive coin cell casing was placed on top and pressure was applied to close the coin cell. The coin cell was then placed into an automatic coin cell-crimping machine, shown in Figure 16.

Figure 16. The MTI compact electric coin cell crimping and disassembling machine was used to seal the coin cells during battery assembly.

The open circuit potential (voltage) of each coin cell was then measured. Functional coin cells were labeled by date of production and catalogued prior to testing (Figure 17).

Figure 17. Once they were assembled and their potential was measured, coin cells were serialized according to date of production.

C. TESTING

Functional coin cells were tested using a MACCOR 4200 battery test system (Figure 18). The MACCOR 4200 battery test system consist of 16 channels capable of delivering ±5 V or 0 to 10 V, a current of 150 µA to 15 A and charge and discharge powers of up to 2400 Watts.

Figure 18. The MACCOR 4200 battery test system was used to test coin cells following battery assembly.

In general, in this study the first series of electrochemical tests for newly produced coin cells included battery conditioning, which consisted of five charge/discharge cycles at a C-rate of C/10. (C-rates will be discussed in more detail in a later section.) The second series of tests included rate testing, which consisted a series of charge/discharge cycles at various C-rates.

III. RESULTS AND DISCUSSION

A. PRODUCTION

1. Objective

The focus of this research revolved around improvement of the existing electrode fabrication methods in order to increase the reproducibility and consistency of battery test results, a basic requirement for the evaluation of new lithium-ion battery materials. The main areas of improvement that were targeted in this research include homogeneity of the electrode films and reproducibility of electrochemical performance.

2. Optimization of Electrode Film Production

Addressing the cracking in the electrode films required modifications to the ratios at which the dry ingredients were mixed and to the amount of solvent used in order to achieve the proper viscosity of slurry for a particular carbon-based anode material. Each material required a different recipe with its own active material-to-additive ratio. Addition of solvent varied based on the density and the dispersion of the ingredient mixture, which varied due differences in porosity, surface area, and agglomeration behavior of the different anode materials. In most cases, the amount of solvent was minimized to produce a thicker slurry.

Laboratory-produced graphite anodes consisted of 77 wt% graphitic carbon, 11.5 wt% PVDF and 11.5 wt% acetylene black. CDC anodes used ~80 wt% CDC (synthesized at 600 °C or 1200 °C) and ~20 wt% PVDF. Carbon onion anodes were produced with 80 wt% carbon onion, 15 wt% PVDF and 5 wt% acetylene black. Lastly, MWCNT anodes used ~80 wt% MWCNT, ~15 wt% PVDF and ~5 wt% acetylene black. With the exception of the ratio provided for MWCNT production, which will be discussed later, the optimal recipes for the anodes produced in this study were summarized earlier in Table 1.

Due to their high porosity and/or increased surface area, carbon materials other than graphitic carbon required the addition of much more PVDF binder in order to reduce cracking and improve adhesion of the slurry to the current collector. Other key improvements included the reduction of solvent added, which yielded thicker slurry, and a reduction in slurry height upon casting. In summary, a thicker slurry was cast into a thinner film onto the current collector. The optimal slurry height during casting, including the foil thickness, was determined to be 1 mm for graphitic carbon and carbon onion and 0.7 mm for TiC-CDC 600 °C and TiC-CDC 1200 °C.

The casting process was also optimized. Instead of pushing the glass with the current collector over another plate of glass under the micrometer adjustable film applicator, a single plate of glass was used. The adjustable film applicator was pushed across the plate of glass on which the current collector had been prepped, eliminating variations in film casting due to varying thicknesses in multiple plates of glass. The casting surface was also precisely leveled to reduce weight fluctuations in the electrode film experienced after drying. Previously, weight fluctuations in electrodes produced in a single film of up to 40 percent of the average electrode weight were experienced. Optimization reduced these weight fluctuations such that electrodes produced from a single electrode film were consistently within 10 percent of average electrode weight. However, it should be noted that the largest fluctuations occurred along the edges of the electrode film, as opposed the center, as was the case in previous electrode fabrication efforts. The result pictured in Figure 19 demonstrates increased homogeneity in the film produced and the elimination of visible cracking, compared to the recipe and method used in Figure 9.

Figure 19. Laboratory-produced electrode film using graphite and optimized fabrication method.

While fabrication of CDC and carbon onion anodes was achieved, there remained some irreconcilable issues with the recipe for the production of MWCNT anodes. Attempts at producing anodes using MWCNT were not successful, as the films yielded excessive cracking upon drying, as shown in Figure 20.

Figure 20. Cracking in MWCNT electrode film was consistently experienced in the fabrication process.

The introduction of solvent to the MWCNT dry mixture was particularly difficult, and obtaining a slurry viscosity close to that of the other materials required nearly twice as much solvent addition (11 mL). The dry ingredients for MWCNT included 840 mg of MWCNT powder, 150 mg of PVDF and 50 mg of acetylene black. Despite variations to the amount of solvent used and the attempt at mixing the dry ingredients in the 8000 M SPEX Sample Prep Mixer/Mill (Figure 21), the cracking the in the MWCNT electrode film could not be eliminated.

Figure 21. 8000 M SPEX Sample Prep Mixer/Mill used to mix dry ingredients for MWCNT electrode film production.

The use of a different binder in the electrode recipe was also attempted. Graphite electrodes using 3 to 5 wt% carboxymethyl cellulose (CMC) binder, in conjunction with de-ionized water in place of NMP solvent, were fabricated. However, the slurries produced could not be adequately mixed by hand or with the addition of ball milling the dry or wet mixture. As a result, the dried films demonstrated high agglomeration and porosity (Figure 22). Adhesion to the current collector was also a problem.

Figure 22. Laboratory-produced electrode films using graphite, CMC binder and de-ionized water contained high levels of agglomeration and subsequent cracking.

3. Addressing Moisture Absorption

Another area of concern included the issue of moisture absorption in the electrodes. Electrodes were fabricated in the ambient environment and subject to moisture and other contaminants. Particular care was taken to isolate the electrodes in order to prevent contamination with other materials, but the issue of moisture and its level of absorption into the individual electrodes had yet to be evaluated. Originally, electrodes were dried in the laboratory oven overnight and then placed into the transfer chamber of the glove box, where they were placed under vacuum prior to being transferred into the glove box. However, it was not clear what method of moisture removal was the most effective.

Consequently, a test was conducted to determine how much moisture electrodes absorb in the ambient environment and which method, drying or placing into vacuum, would be the best method of moisture removal. Two sets of electrodes were used in this experiment. One set had been placed in the

laboratory oven overnight. The other was placed under vacuum in the glove box transfer chamber for 30 minutes. Each set was then removed from its drying location and weighed every ten seconds over the course of 15 minutes in order to observe increases in electrode weight due to moisture absorption. The results from this experiment are plotted in Figure 23.

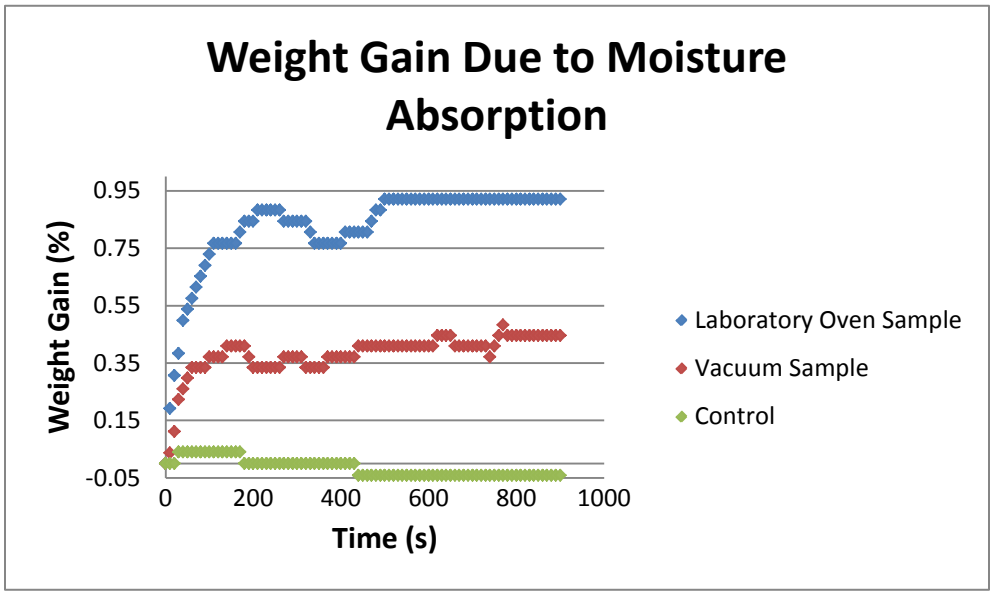

Figure 23. Weight gain due to moisture absorption over 15 minutes. The laboratory oven sample demonstrated the highest percentage weight gain over time.

The laboratory oven sample set experienced the highest amount of weight gain over time, settling at just under one percent weight gain. The vacuum sample set experienced around a half-percent weight gain. Of note, the highest amount of weight gain due to moisture absorption occurred within the first two minutes of placement into ambient conditions.

Although the weight gain in the electrodes due to moisture occurred in what seems to be small percentages, the goal was to eliminate any moisture absorption possible. Moisture in the internal components of the cell can significantly decrease cell capacity. All subsequent electrodes were placed into

the laboratory oven to dry overnight. Once they were removed from the laboratory oven, they were immediately placed under vacuum prior to battery assembly.

4. Cutting Electrodes from the Electrode Film

Another source of inconsistency was the method by which electrodes were cut from the electrode film. Originally, the electrodes were punched out of the film by hand with a non-sparking hammer (Figure 24).

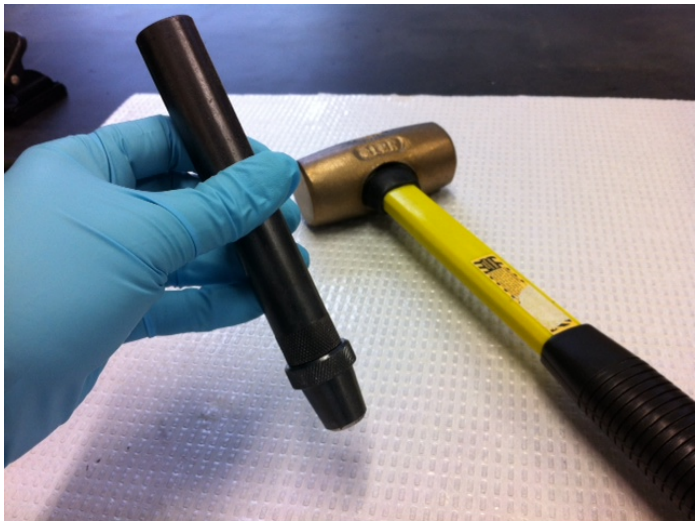

Figure 24. Electrodes were originally punched from the electrode film by hand.

As a result, individual electrodes experienced varying levels of damage around the edges, and there were problems with film adherence to the current collector (Figure 25).

Figure 25. Damage experienced by a graphite-based electrode film due to punching out electrodes by hand.

There were also problems with variations in electrode diameter and weight fluctuations due to excessive cracking. The use of the disc cutter (see Figure 13) alleviated these issues and created consistently sized electrodes with minimal damage, as shown in Figure 26.

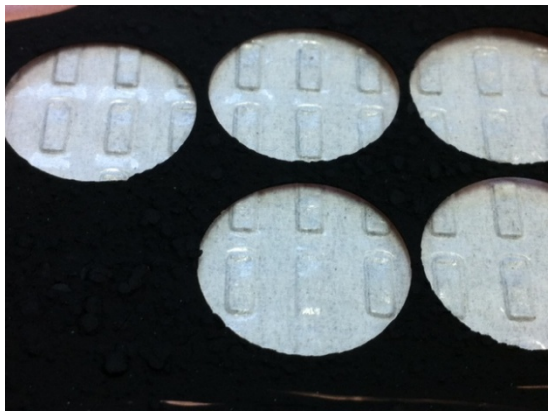

Figure 26. Damage to the electrode film using the MTI disc cutter was minimal.

The production of lithium-ion battery anodes then achieved an increased degree of consistency and reproducibility. However, verification of the improvements to the lithium-ion battery anode fabrication methods required battery testing.

B. TESTING

1. Overview

The MACCOR 4200 battery test system was used to verify the electrochemical performance of the coin cells produced for this research. Initially, the coin cells underwent conditioning, which consists of cycling through five charge/discharge cycles at a constant current. Lithium-ion batteries are typically cycled between 3.0 and 4.2 V. This process was conducted at different C-rates, which describe the capacity rating of the battery in terms of battery charging.

The capacity of the battery is determined based on the weight of the active material used. In the case of this study, the active material was graphite, CDC or carbon onion. For instance, if a battery's capacity is determined to be 3.61 mAh, charging the battery at a C-rate of 1C would require a current of 3.61 mA. At this current, it would take 1 hour to charge and 1 hour to discharge the battery. Using a C-rate of C/10 would require a current of 361μA, and it would take 10 hours to charge and 10 hours to discharge the battery [4]. The goal is obtaining consistency with the calculations based on the active material weight of the electrodes.

2. Commercial Graphitic Carbon-Based Coin Cells

To establish a baseline and verify success of the optimization of the electrode fabrication method, coin cells produced using commercial graphitic carbon-based anodes were tested first. Their initial testing involved cycling the coin cells five times at a C/10 rate.

The initial charge in the first charge/discharge cycle depicts formation of the solid electrolyte interphase (SEI) layer. The SEI layer is essential to the life of the battery because it prevents further reaction with the electrolyte. During the initial charge, the electrolyte reacts with the anode to form the passivating SEI layer, which moderates the charge rate and restricts current. However, its

formation contributes to irreversible capacity because it consumes a large amount of lithium ions during this process [5].

Five charge/discharge cycles for a coin cell produced using a commercial graphite anode and a $LiCoO_2$ cathode are shown in Figure 27.

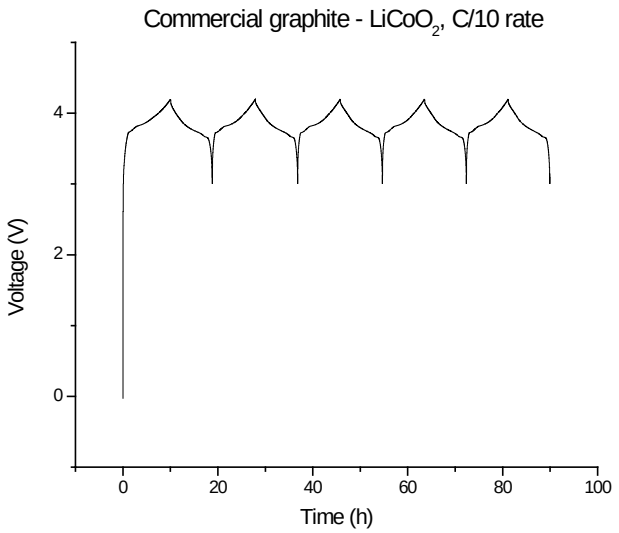

Figure 27. Five charge/discharge cycles of a commercial graphite - $LiCoO_2$ coin cell (charge current: 361 µA, charge capacity from third cycle: 3.28 mAh, discharge capacity from third cycle: 3.214 mAh, specific capacity: 236.8 mAh/g). The charge in the first cycle depicts formation of the SEI layer.

Note that there is a difference between charge and discharge in the first cycle due to SEI layer formation. The SEI layer is stabilizes after several cycles, and the specific charge and discharge capacity values level out. The formation of the SEI layer creates varying degrees of irreversible capacity, the magnitude of which depends on the electrode material. This behavior was more prominent with other anode materials, which will be discussed later in this section. The cells fabricated had an excess of anode material. Thus, the cells were limited by the capacity of the cathode, which in this case, was the $LiCoO_2$ cathode. The specific capacity of the $LiCoO_2$ cathode, according to the manufacturer, MTI Corporation, is 145 mAh/g.

The mass of the active material is determined precisely in the development of prototype anodes and cathodes. The volume, however, is an estimate based upon an approximate tap density. As a result, performance is more accurately described in terms of specific capacity and specific energy, which are derived from a measured charge and voltage normalized by a known mass. The energy density of the electrodes, on the other hand, is normalized by the electrode volume.

3. Laboratory-Produced Graphitic Carbon-Based Coin Cells

The next set of cells produced were laboratory-produced graphite - $LiCoO_2$ coin cells. Again, the formation of the passivating SEI layer is evident during the charging portion of the first cycle (Figure 28).

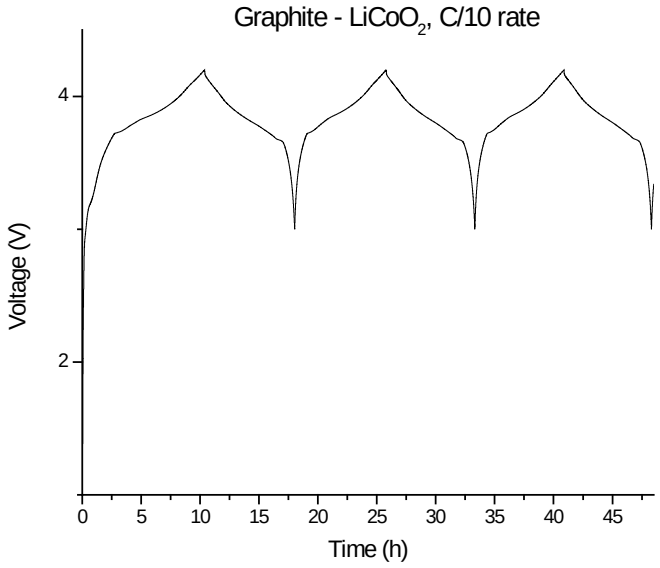

Figure 28. The first three charge/discharge cycles of a laboratory-produced graphite - $LiCoO_2$ coin cell (charge current: 361 µA, charge capacity from third cycle: 2.73 mAh, discharge capacity from third cycle: 2.68 mAh, specific capacity: 235.7 mAh/g). The charge in the first cycle depicts formation of the SEI layer

The specific capacity is based off the discharge capacity divided by the active material weight of the graphitic carbon-based anode. Note the near-symmetric, gradual slope of the charge/discharge curves in Figures 26 and 27, which are characteristic of the voltage profile corresponding to the lithiation and delithiation processes at the cathode.

Multiple graphite - $LiCoO_2$ coin cells composed of anodes originating from a single electrode film were also cycled at C/10 in order to verify reproducibility. Figure 29 illustrates the reproducibility of results from electrochemical testing. The initial charge/discharge cycle for the four coin cells produced similar voltage profiles occurring over approximately the same period. Deviations in subsequent cycles have slight variations in time, but the voltage profiles are retained.

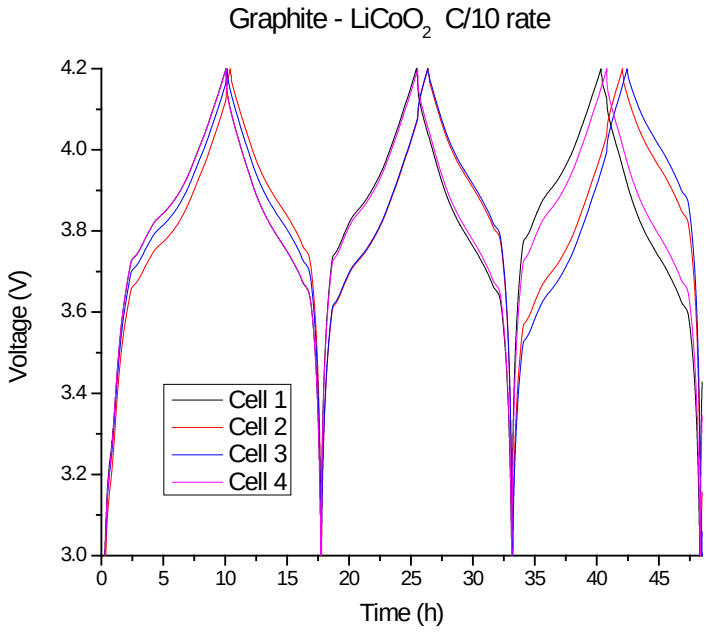

Figure 29. The first three charge/discharge cycles of four laboratory-produced graphite - $LiCoO_2$ coin cells composed of anodes originating from a single electrode film (charge current: 361 µA).

Rate testing was also conducted on the graphite - $LiCoO_2$ coin cells with three cycles each at the following rates: C/20, C/10, C/8, C/5, C/3, C/2 and 1C. Figure 30 depicts the capacity of the cell as a function of the number of cycles. The specific charge and discharge capacity starts at 258.5 mAh/g and 237.7 mAh/g, respectively, at a rate of C/20, diminishing to 23.25 mAh/g and 23.27 mAh/g at 1C. This effect can be attributed to mass transport limitations at the electrodes. It is also much more prominent at higher C-rates, illustrating the power limitations of graphite. The battery was already cycled prior to rate testing and therefore shows no signs of SEI layer formation.

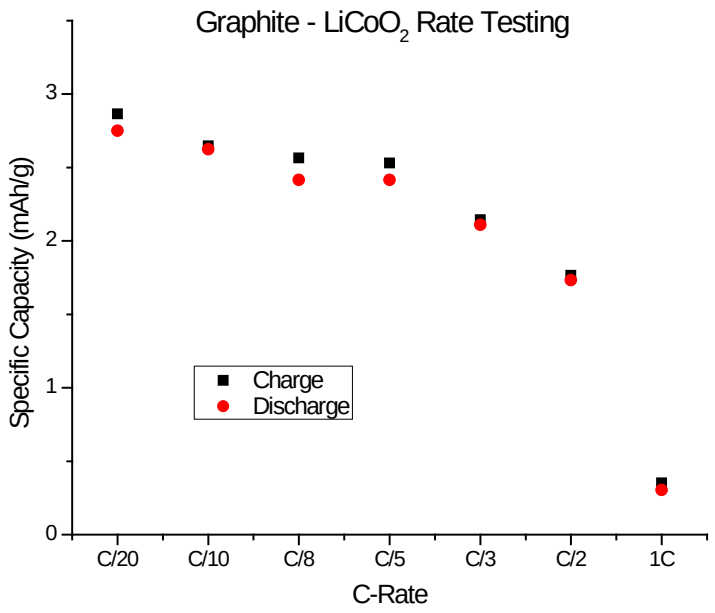

Figure 30. Specific capacity (mAh/g) at various C-rates during rate testing of graphite - $LiCoO_2$ coin cells.

4. Graphite - Lithium Metal Half-Cells

Half-cells composed of commercial graphite and lithium metal and laboratory-produced graphite and lithium metal were assembled and tested, as well. Notice the voltage profile in both the commercial graphite and laboratory-

produced graphite versus lithium metal (Figures 31 and 33). Both exhibit flatter profiles near the peaks, demonstrating behavior characteristic to the intercalation and deintercalation process of graphite. Figure 32 illustrates the specific capacity of commercial graphite versus lithium metal by cycle number. The specific charge and discharge capacities at C/20 are 327.8 mAh/g and 327.1 mAh/g, respectively, diminishing to 2.48 mAh/g and 2.69 mAh/g. Of note, the commercial graphite - lithium metal half-cells start with the highest specific charge and discharge capacities, but they also experience the largest drop in specific charge and discharge capacity with increasing C-rates, compared to the other materials used in this study.

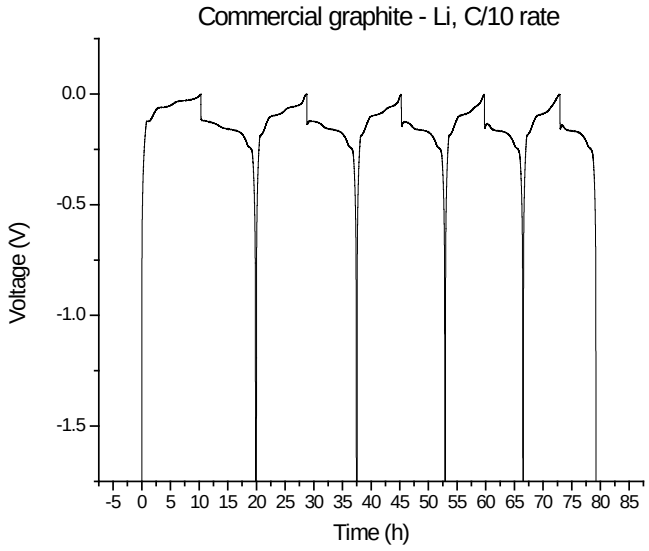

Figure 31. The first five charge/discharge cycles of an MTI commercial graphite - lithium metal half-cell (charge current: 361 µA, charge capacity from third cycle: 3.48 mAh, discharge capacity from third cycle: 3.44 mAh, specific capacity: 253.5 mAh/g).

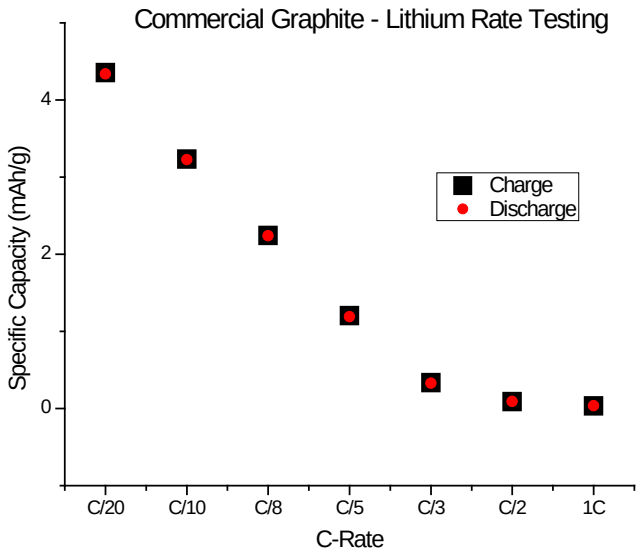

Figure 32. Specific capacity (mAh/g) at various C-rates during rate testing of commercial graphite - lithium metal half-cells.

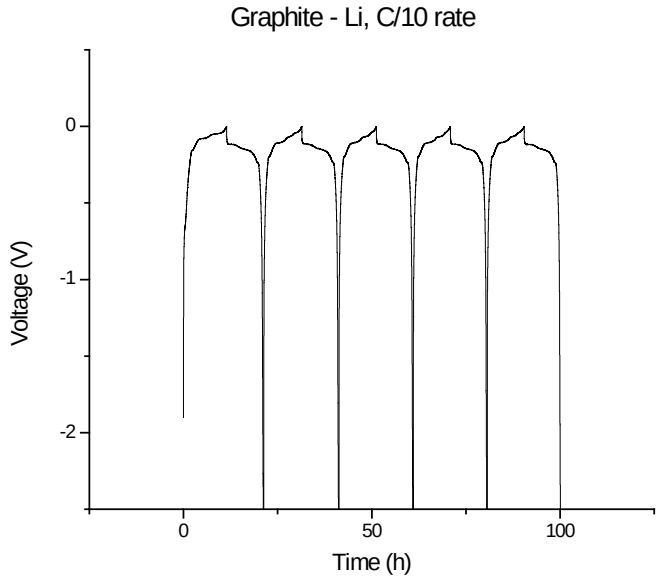

Figure 33. The first five charge/discharge cycles of a laboratory-produced graphite - lithium metal half-cell (charge current: 420 µA, charge capacity from third cycle: 4.18 mAh, discharge capacity from third cycle: 4.11 mAh, specific capacity: 330.4 mAh/g).

5. TiC-CDC 1200 °C - Li Metal Half-Cells

As seen in the HRTEM micrograph in Figure 34, TiC-CDC 1200 °C has a much higher degree of ordering than the highly amorphous TiC-CDC 600 °C shown in Figure 38. The micrograph depicts significant layering and stacking, indicating the occurrence of graphitization.

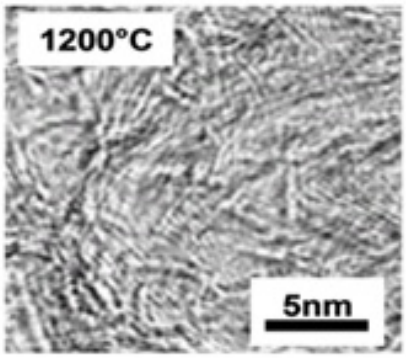

Figure 34. HRTEM micrograph of TiC-CDC 1200 °C depicting graphitization (From [11]).

This fact, coupled with the use of lithium metal vice $LiCoO_2$, greatly reduces the consumption of lithium ions during the initial charge formation of the passivating SEI layer. Thus, the resulting charge/discharge curves for TiC-CDC 1200 °C – lithium metal did not reflect the same excessive consumption of lithium ions in the initial charge formation of the SEI layer (Figure 35). Replacement of the $LiCoO_2$ cathode with lithium metal also changes the voltage range during the cycling process to -3.0 V to 0 V vs. Li/Li^+. In contrast to the TiC-CDC 600 °C – $LiCoO_2$ cell, the SEI layer formation in the TiC-CDC 1200 °C - lithium metal sample had much less effect on specific capacity, the latter yielding 202.4 mAh/g vice the former's 43.85 mAh/g.

Rate testing data (Figure 36) exhibits the same diminishing specific capacity characteristics as seen before.

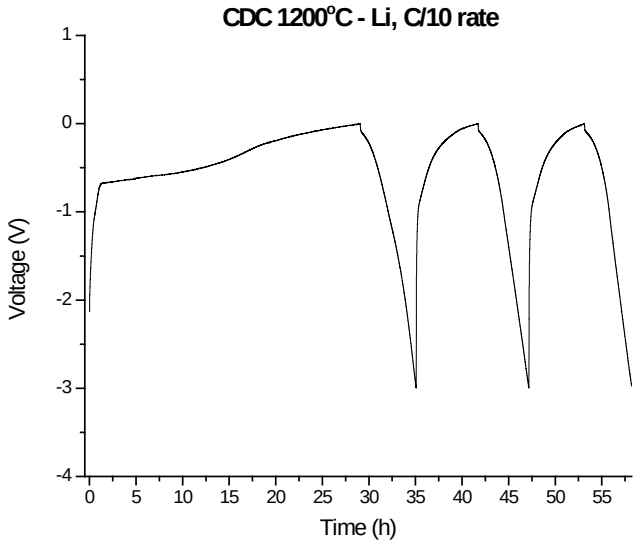

Figure 35. The first three charge/discharge cycles of a TiC-CDC 1200 °C - lithium metal half-cell (charge current: 530.5 µA, charge capacity from third cycle: 3.520 mAh, discharge capacity from third cycle: 2.907 mAh, specific capacity: 202.4 mAh/g).

The specific charge capacity is generally greater than the specific discharge capacity, but their values converge upon stabilization after many cycles. Again, the diminishing specific charge and discharge capacities are evident as the C-rate increases. The first cycle yields a specific charge and discharge capacity of 222.8 mAh/g and 204.8 mAh/g, respectively. At 1C, these specific charge and discharge capacities drop to 20.04 mAh/g and 20.06 mAh/g.

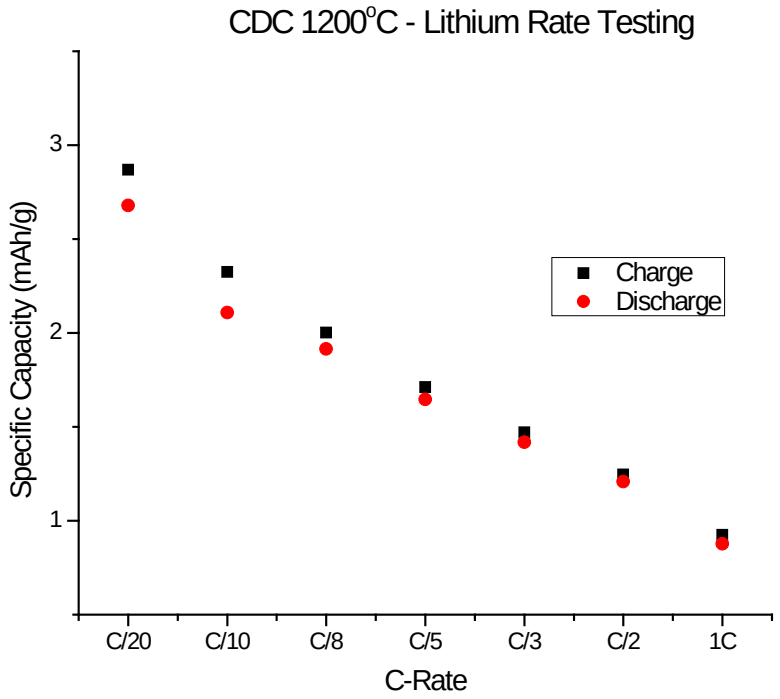

Figure 36. Specific capacity (mAh/g) at various C-rates during rate testing of TiC-CDC 1200 °C - lithium metal half-cells.

6. TiC-CDC 600 °C - $LiCoO_2$ Coin Cells

The next set of cells tested were made with TiC-CDC 600 °C anodes and $LiCoO_2$ cathodes. The formation of the SEI layer exhibited in the initial charge was much more pronounced in these cells (Figure 37). Notice the continuously sloping voltage profile upon charge and discharge. TiC-CDC 600 °C, unlike graphite, does not experience conventional intercalation/deintercalation reactions.

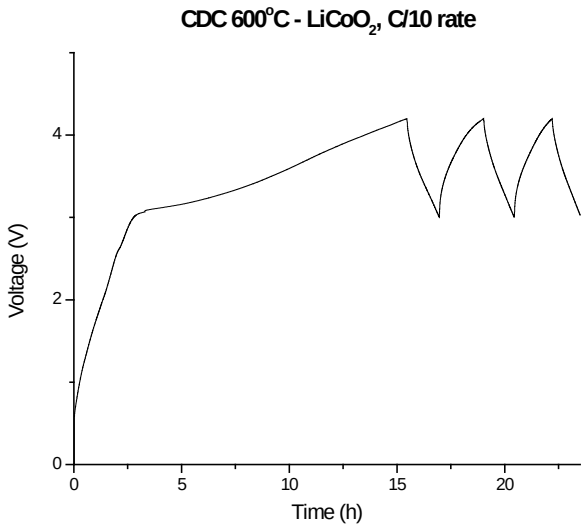

Figure 37. The first three charge/discharge cycles of a TiC-CDC 600 °C – $LiCoO_2$ cell (charge current: 361 µA, charge capacity from third cycle: 0.650 mAh, discharge capacity from third cycle: 0.469 mAh, specific capacity: 43.85 mAh/g). This cell has a very pronounced initial charge curve, indicating the SEI layer formation has consumed a large number of lithium ions.

The first curve demonstrates the SEI layer formation consumes a large amount of Li ions that cannot be recovered. This behavior is also reflected in its low specific capacity (43.85 mAh/g) in subsequent cycles. There are two possible reasons for this particular behavior. TiC-CDC 600 °C is a highly amorphous material, as shown in the HRTEM micrograph (Figure 38). Second, the use of $LiCoO_2$ does not provide as much lithium ions as lithium metal.

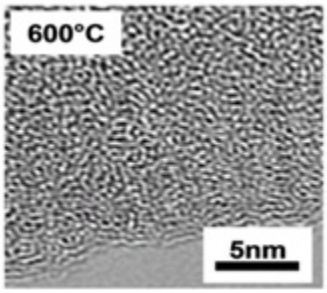

Figure 38. HRTEM micrograph of highly amorphous TiC-CDC 600 °C (From [11]).

Thus, the half-cells using TiC-CDC 1200 °C and lithium metal, which has a much higher supply of lithium ions than $LiCoO_2$, demonstrated the consumption of lithium ions during the formation of the SEI layer did not create such a dramatic decrease to the specific capacity as experienced in the TiC-CDC 600 °C- $LiCoO_2$ coin cells.

7. Carbon Onion - Lithium Metal Half-Cells

The cycle testing results for a carbon onion - lithium metal half-cell are depicted in Figure 39.

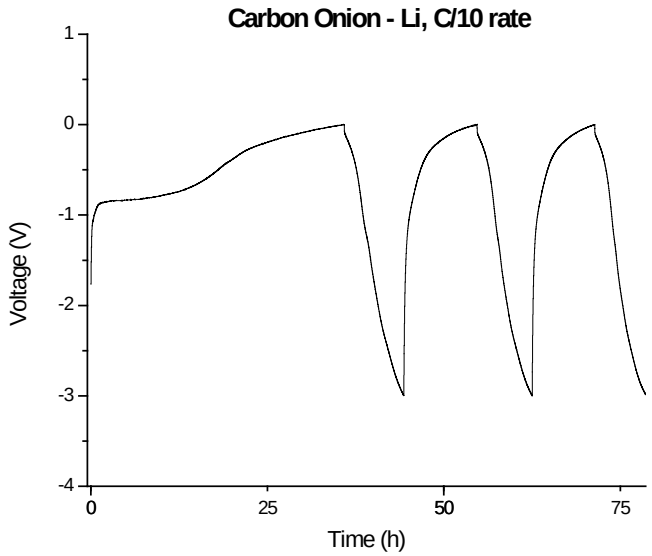

Figure 39. The first three charge/discharge cycles of a carbon onion - lithium metal half-cell (charge current: 628 µA, charge capacity from third cycle: 6.51 mAh, discharge capacity from third cycle: 4.91 mAh, specific capacity: 299.8 mAh/g).

The specific capacity was calculated to be 299.8 mAh/g, a much higher value than all the other laboratory-produced materials used in this study.

IV. SUMMARY AND CONCLUSION

This thesis is a continuation of the newly established battery research at NPS. Previous work done by LT Kamryn Sakamoto set the groundwork for the fabrication of lithium-ion battery electrodes, but left adequate room for improvement of processes [15]. The evaluation of new carbon nanomaterial-based lithium-ion battery anodes requires consistent, reproducible test data, which in turn is based on an optimized electrode fabrication process.

Thus, the primary focus of this study was to improve the electrode fabrication process such that cell-to-cell variations in electrochemical performance are minimized. Furthermore, the suitability of the developed fabrication process for other carbon nanomaterials has been evaluated.

Alterations to the electrode fabrication process addressed several important issues, such as the homogeneity and reproducibility of the electrodes. Changes were made in mixing, casting and cutting. Ratios of electrode film components were optimized, and concerns over electrode moisture absorption were addressed. The results of this study were improved homogeneity of electrode films with minimal weight fluctuations and improved reproducibility of electrochemical performance.

Once the fabrication was optimized for CDC, the process was utilized for other carbon nanomaterials, including carbon onion and MWCNTs. While the quality of carbon onion-based anodes was similar to that of CDC electrodes, the quality of MWCNT electrodes was insufficient and did not allow for electrochemical testing. The MWCNT electrode films were subject to extreme cracking and porosity. Yet more improvements can be made to the electrode fabrication process.

Follow-up studies will continue electrochemical testing of the CDC and carbon onions to collect sufficient data for publication in a peer-reviewed journal. There is also room for exploration of other CDC materials (besides the TiC-CDC

600 °C and TiC-CDC 1200 °C) to obtain a more robust set of data and deeper understanding of the charge storage mechanism.

Furthermore, experimenting with different binders may prove useful, particularly for MWCNT. This study briefly explored the use of CMC binder and de-ionized water in place of PVDF and NMP solvent. However, the agglomeration and cracking in the electrode film could not be eliminated, possibly due to insufficient mixing. A roller mixer has been purchased and will be used for future electrode fabrication.

Nonetheless, in the scope of this research, achieving consistent data through electrochemical testing has successfully been demonstrated. Commercial and laboratory-produced graphite anodes, paired with $LiCoO_2$ or lithium metal, were successfully cycled and rate tested, as were anodes consisting of TiC-CDC (600 °C and 1200 °C) and carbon onion. Half-cells of carbon onion and lithium metal displayed a very high specific capacity (299.8 mAh/g), second only to the specific capacity calculated from the commercial graphite - lithium metal (330.4 mAh/g). These results suggest the feasibility of the use of carbon nanomaterials in lithium-ion batteries. When paired with lithium metal, the TiC-CDC 1200 °C anodes had a specific capacity of approximately 20 mAh/g at 1C, compared to less than 3 mAh/g at 1C for commercial graphite - lithium metal half-cells, suggesting far superior power performance. Although in comparison the average specific capacities of TiC-CDC 1200 °C samples were much lower than those of commercial graphite, the commercial graphite's large decrease in specific capacity over the equivalent C-rates demonstrated the inferior power characteristics of graphite.

In summary, this study further advanced the battery research capabilities at NPS, paving the way for more extensive electrochemical testing to take place. There is still much to discover in drawing connections between the various structural features of highly amorphous CDCs and other carbon nanomaterials and electrochemical performance. Yet more improvements can be made to the electrode fabrication process, including experiments with different binders or

developing a more precise method for application of electrolyte. Additional electrochemical testing with amorphous carbons and carbon nanomaterials on a larger scale can also be conducted as a basis for publication.

THIS PAGE INTENTIONALLY LEFT BLANK

LIST OF REFERENCES

[1] Naval Sea Systems Command Public Affairs. (2011, December 9). *LCAC 91 Achieves Navy's fastest maritime surface craft speed on algal fuel*. [Online]. Available: http://www.navy.mil/search/display.asp?story_id=64290.

[2] C. Liu et al., "Advanced materials for energy storage," *Advanced Energy Materials,* vol. 22, pp. E28-E62, 2010.

[3] Woodbank Communications Ltd. (2005). *Battery performance characteristics*. [Online]. Available http://www.mpoweruk.com/performance.htm.

[4] J. Farmer et al., "Special Topics in Energy Conversion and Storage," ME4901, LLNL-MI-464396, LLNL, Livermore, CA, 2010.

[5] *Handbook of Batteries*, 3rd ed., McGraw-Hill Professional, New York, NY, 2001.

[6] J. Voelcker. (2007, September). *Lithium batteries take to the road*. [Online]. Available: http://spectrum.ieee.org/green-tech/advanced-cars/lithium-batteries-take-to-the-road/2.

[7] Q. Hu et al., "Graft copolymer-based lithium-ion battery for high-temperature operation," *J. Power Sources,* vol. 196, pp. 5604–5610, 2011.

[8] Author Unknown. (n.d). *High-pressure transformations of single-crystal graphite.* [Online]. Available: http://rruff.geo.arizona.edu/OLA/files/SXD/graphite.htm.

[9] M. Endo et al., "Recent development of carbon materials for Li-ion batteries," *Carbon,* vol. 38, pp. 183–197, 1999.

[10] R. Dash et al., "Titanium carbide derived nanoporous carbon for energy-related applications," *Carbon,* vol. 44, pp. 2489–2497, 2006.

[11] *Nanomaterials Handbook*, 1st ed., CRC Press, Philadelphia, PA, 2006.

[12] Q. Zou et al., "Characterisation of onion-like carbon fabricated by annealing nanodiamond," *Materials Research Innovations,* vol. 14, no. 4, pp. 285–288, 2010.

[13] Z. J. Qiao et al., “Graphitization and microstructure transformation of nanodiamond to onion-like carbon,” *Scripta Materialia,* vol. 54, no. 2, pp. 225–229, 2006.

[14] B. J. Landi et al., “Carbon nanotubes for lithium-ion batteries,” *Energy and Environmental Sci.,* vol. 2, no. 6, pp. 638–654, 2009.

[15] K. Sakamoto, “Development of nanoporous carbide-derived carbon electrodes for high-performance lithium-ion batteries,” M.S. thesis, Department of Mechanical and Aerospace Engineering, Naval Postgraduate School, Monterey, CA, 2011.

INITIAL DISTRIBUTION LIST

1. Defense Technical Information Center
   Ft. Belvoir, Virginia

2. Dudley Knox Library
   Naval Postgraduate School
   Monterey, California

3. Sebastian Osswald
   Naval Postgraduate School
   Monterey, California

4. Joseph Farmer
   Lawrence Livermore National Laboratory
   Livermore, California &
   Naval Postgraduate School
   Monterey, California